toroidal and a poloidal field of the same magnitude exist. Our estimates of the dynamo Joule dissipation suggest that the lower oceanic layer is slightly preferred because of a good compromise between a large radius and low resistivity.

We also can consider applying the scaling law for a Busse dynamo. Here we must note that other dynamo models generally address planetary fields with small tilts. For a Busse dynamo, the dipole moment is proportional to R^4, where R is the radius of the conducting dynamo region. With a rotation period of 17.3 hours for Uranus and calibration of the constant at Earth, we find that a dynamo in the lower "oceanic" part of Uranus is also most consistent with our results.

The possibility that we may be observing a polarity reversal, well known for the case of the terrestrial magnetic field (*34*) or the more general case of a nonsteady dynamo (*35*), cannot be ignored; the relatively large quadrupole components implied in our initial OTD field representation suggest that we consider this possibility. The observed large offset of the equivalent dipole is a question about which we can only speculate. Does it mean that the interior structure departs substantially from spherical symmetry? Or is it only the dynamo system that does? Is this due to a catastrophic collisional event subsequent to the formation of the planet, intimately related to its large and anomalous obliquity to the ecliptic? The continued study of these data may provide clues to the answer.

REFERENCES AND NOTES

1. K. W. Behannon *et al.*, *Space Sci. Rev.* **21**, 235 (1977).
2. N. F. Ness *et al.*, *Science* **206**, 966 (1979); N. F. Ness *et al.*, *ibid.* **215**, 558 (1982).
3. N. F. Ness, M. H. Acuña, K. W. Behannon, F. M. Neubauer, *J. Geophys. Res.* **87**, 1369 (1982).
4. M. L. Kaiser and M. D. Desch, personal communication; J. W. Warwick *et al.*, *Science* **233**, 102 (1986).
5. J. T. Clarke, *Astrophys. J.* **263**, L105 (1982); S. T. Durrance and H. W. Moos, *Nature (London)* **299**, 428 (1982); J. T. Clarke *et al.*, *Bull. Am. Astron. Soc.* **17**, 745 (1985).
6. R. V. Yelle and B. R. Sandel, *Geophys. Res. Lett.* **13**, 89 (1986).
7. G. L. Siscoe, *Planet. Space Sci.* **19**, 483 (1971); *Icarus* **24**, 311 (1975).
8. T. W. Hill, A. J. Dessler, M. E. Rassbach, *Planet. Space Sci.* **31**, 1187 (1983).
9. G.-H. Voigt, T. W. Hill, A. J. Dessler, *Astrophys. J.* **266**, 390 (1983).
10. T. W. Hill, in *Uranus and Neptune*, J. T. Bergstrahl, Ed. (*NASA Conf. Publ. 2330*, 1984), p. 497.
11. ——— and A. J. Dessler, *Science* **227**, 1466 (1985).
12. S. A. Curtis and N. F. Ness, *Geophys. Res. Lett.* **12**, 855 (1985).
13. H. S. Bridge *et al.*, *Science* **233**, 89 (1986).
14. J. T. Choe, D. B. Beard, E. C. Sullivan, *Planet. Space Sci.* **21**, 485 (1973).
15. D. H. Fairfield, *J. Geophys. Res.* **76**, 6700 (1971).
16. J. A. Slavin, R. E. Holzer, J. R. Spreiter, S. S. Stahara, D. S. Chanssee, *ibid.* **88**, 19 (1983).
17. J. A. Van Allen, in *Highlights of Astronomy*, E. A. Müller, Ed. (International Astronomical Union, Paris, 1977), vol. 4, part 1, pp. 195–224.
18. M. H. Acuña and N. F. Ness, *J. Geophys. Res.* **81**, 2917 (1976); E. J. Smith, L. Davis, Jr., D. E. Jones, in *Jupiter*, T. Gehrels, Ed. (Univ. of Arizona Press, Tucson, 1976), p. 788; E. J. Smith *et al.*, *J. Geophys. Res.* **85**, 5655 (1980); J. E. P. Connerney, N. F. Ness, M. H. Acuña, *ibid.* **88**, 8771 (1983).
19. D. H. Fairfield, *J. Geophys. Res.* **85**, 775 (1980).
20. S. J. Bame, J. R. Asbridge, H. E. Felthauser, E. W. Hones, I. B. Strong, *ibid.* **72**, 113 (1967).
21. K. W. Behannon, *ibid.* **73**, 907 (1968); J. D. Mihalov, D. S. Colburn, R. G. Currie, C. P. Sonett, *ibid.*, p. 943; J. A. Slavin, B. T. Tsurutani, E. J. Smith, D. E. Jones, D. G. Sibeck, *Geophys. Res. Lett.* **10**, 973 (1983).
22. G. D. Mead and W. N. Hess, *J. Geophys. Res.* **78**, 2793 (1973).
23. C. E. McIlwain, *ibid.* **66**, 3681 (1961).
24. E. C. Stone *et al.*, *Science* **233**, 93 (1986); S. M. Krimigis, *ibid.*, p. 97.
25. A. F. Cheng, in *Uranus and Neptune*, J. T. Bergstrahl, Ed. (*NASA Conf. Publ. 2330*, 1984), p. 541.
26. F. M. Neubauer, *J. Geophys. Res.* **85**, 1171 (1980).
27. N. F. Ness, in *Solar Terrestrial Physics/1970*, E. R. Dyer, Ed. (Reidel, Dordrecht, Netherlands, 1972), part 2, pp. 159–205.
28. G. Schubert and K. Schwartz, *Moon* **1**, 106 (1969); C. P. Sonett, B. F. Smith, D. S. Colburn, G. Schubert, K. Schwartz, *Proc. Lunar Sci. Conf.* **3**, 2309 (1972).
29. M. Torbett and R. Smoluchowski, *Nature (London)* **286**, 237 (1980).
30. W. B. Hubbard, in *Uranus and Neptune*, J. T. Bergstrahl, Ed. (*NASA Conf. Publ. 2330*, 1984), p. 291.
31. E. N. Parker, *Astrophys. J.* **122**, 293 (1955).
32. A. C. Mitchell and W. J. Nellis, *J. Chem. Phys.* **76**, 6273 (1982).
33. F. H. Busse, *Phys. Earth Planet. Int.* **12**, 350 (1976).
34. M. D. Fuller, J. W. Williams, K. I. Hoffman, *Rev. Geophys. Space Phys.* **17**, 179 (1979).
35. D. J. Stevenson, *Rep. Prog. Phys.* **46**, 555 (1983).

36. We thank our colleagues at Goddard, those involved with the Voyager CRS, LECP, PLS, and PRA investigations, and S. A. Curtis, D. J. Stevenson, and J. A. Van Allen for discussions of these results. We also thank the entire Voyager project staff at the Jet Propulsion Laboratory, especially G. Sisk, E. Franzgrote, N. Toy, H. Woo, O. Divers, and W. McDougal, for the success of the mission and their support of our investigation; W. Mish and his data processing and analysis team, particularly T. Vollmer, P. Harrison, J. Jones, T. Carleton, J. Annen, G. Burgess, J. Byrnes, S. Kempler, L. Moriarty, F. Ottens, A. Silver, and R. Thompson, for support; C. Moyer, J. Scheifele, J. Seek, and E. Worley for contributions to the design, development, and testing of the hardware; and F. Hunsaker and L. White for technical assistance. F.M.N. was supported financially by the German Ministry of Science and Technology.

2 April 1986; accepted 5 May 1986

Plasma Observations Near Uranus: Initial Results from Voyager 2

H. S. BRIDGE, J. W. BELCHER, B. COPPI, A. J. LAZARUS, R. L. MCNUTT, JR., S. OLBERT, J. D. RICHARDSON, M. R. SANDS, R. S. SELESNICK, J. D. SULLIVAN, R. E. HARTLE, K. W. OGILVIE, E. C. SITTLER, JR., F. BAGENAL, R. S. WOLFF, V. M. VASYLIUNAS, G. L. SISCOE, C. K. GOERTZ, A. EVIATAR

Extensive measurements of low-energy positive ions and electrons in the vicinity of Uranus have revealed a fully developed magnetosphere. The magnetospheric plasma has a warm component with a temperature of 4 to 50 electron volts and a peak density of roughly 2 protons per cubic centimeter, and a hot component, with a temperature of a few kiloelectron volts and a peak density of roughly 0.1 proton per cubic centimeter. The warm component is observed both inside and outside of $L = 5$, whereas the hot component is excluded from the region inside of that L shell. Possible sources of the plasma in the magnetosphere are the extended hydrogen corona, the solar wind, and the ionosphere. The Uranian moons do not appear to be a significant plasma source. The boundary of the hot plasma component at $L = 5$ may be associated either with Miranda or with the inner limit of a deeply penetrating, solar wind–driven magnetospheric convection system. The Voyager 2 spacecraft repeatedly encountered the plasma sheet in the magnetotail at locations that are consistent with a geometric model for the plasma sheet similar to that at Earth.

BEFORE THE VOYAGER 2 FLYBY, nothing was known about the plasma environment of Uranus or about the interaction between the planet and the solar wind. Various speculative models had been proposed (*1–6*) that were based on differing assumptions about plasma processes and on estimates of the planetary magnetic field that ranged from 0 G to more than 10 G. We now describe Voyager 2's observations of the spatial distribution and physical properties of the plasma near Uranus.

The Voyager plasma science (PLS) experiment (*7*) detects positive ions and electrons with energies-per-charge from 10 V to 6 kV. Figure 1 shows an overview of ion and electron fluxes measured near Uranus along the spacecraft trajectory, which is il-

H. S. Bridge, J. W. Belcher, B. Coppi, A. J. Lazarus, R. L. McNutt, Jr., S. Olbert, J. D. Richardson, M. R. Sands, R. S. Selesnick, J. D. Sullivan, Center for Space Research, Massachusetts Institute of Technology, Cambridge, MA 02139.
R. E. Hartle, K. W. Ogilvie, E. C. Sittler, Jr., NASA–Goddard Space Flight Center, Greenbelt, MD 20771.
F. Bagenal, Imperial College, London, England.
R. S. Wolff, Jet Propulsion Laboratory, California Institute of Technology, Pasadena, CA 91109.
V. M. Vasyliunas, Max-Planck-Institüt für Aeronomie, Katlenburg-Lindau, Federal Republic of Germany.
G. L. Siscoe, Department of Atmospheric Science, University of California, Los Angeles, CA 90024.
C. K. Goertz, Department of Physics and Astronomy, University of Iowa, Iowa City, IA 52242.
A. Eviatar, Department of Geophysics and Planetary Sciences, Tel Aviv University, Tel Aviv, Israel.

lustrated in Fig. 2. Uranus is found to have a fully developed magnetosphere, with a bow shock, a well-defined magnetopause, a complicated plasma structure closer to the planet, and an extended magnetotail on the nightside (*8–10*). Our results concern (i) the locations of the bow shock and the magnetopause, (ii) the properties of plasma in the inner magnetosphere, (iii) the configuration of the plasma sheet in the magnetotail, and (iv) possible plasma sources and transport mechanisms.

Bow shock and magnetopause. The times and solar wind conditions of the bow shock and magnetopause crossings by Voyager 2 are listed in Table 1; the locations of the bow shock and magnetopause are plotted in Fig. 2 together with models representing their surfaces. The model curves are conic sections fitted to the first three boundary crossings and constrained in shape to agree with gas-dynamic analogs (*11*). The asymptotic width of the magnetotail is roughly 2.5 times the distance to the subsolar point; thus the shape of the model magnetosphere is blunter than that at Earth but similar to that at Jupiter and at Saturn. The solar wind ram pressure of 1.8×10^{-10} dyne cm^{-2} observed just before the first bow shock crossing and the observed standoff distance of 18.04 Uranus radii (R_U) correspond to a pressure balance with a planetary magnetic

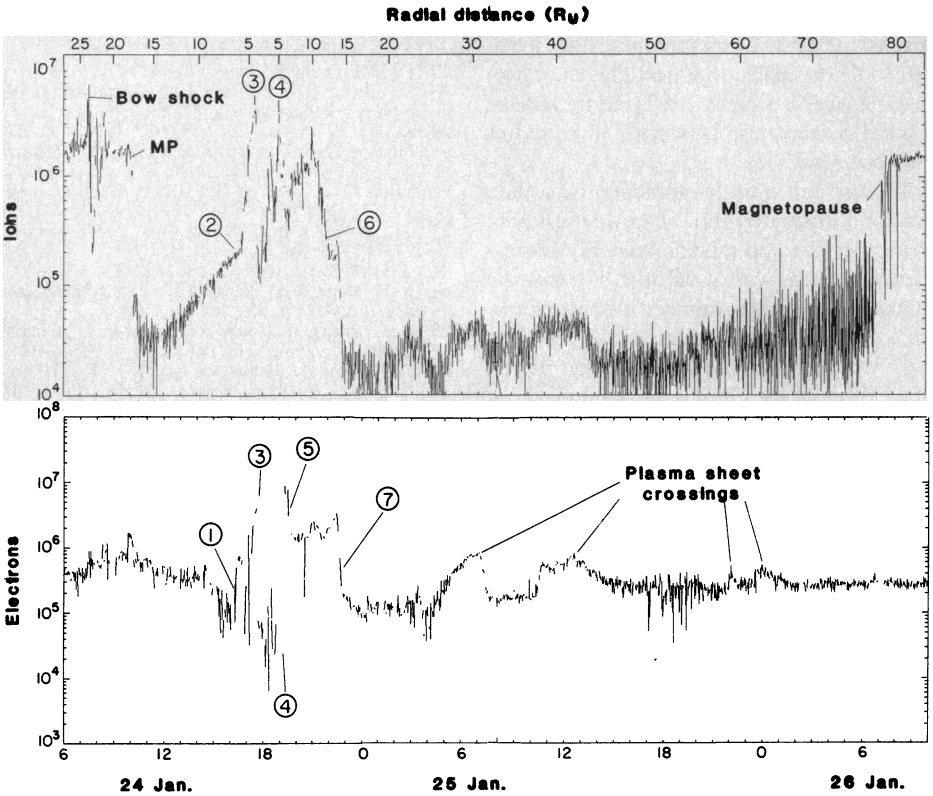

Fig. 1. Profiles of ion (top) and electron (bottom) fluxes (energy range, 10 eV to 1 keV for ions and 120 eV to 6 keV for electrons) measured by the PLS experiment along Voyager 2's trajectory through the magnetosphere of Uranus; unit for flux is particles per square centimeter per second. The circled numerals indicate features discussed in the text (key in legend to Fig. 4). All results are based on fluxes observed above 6×10^4 cm^{-2} sec^{-1} (ions) and 2×10^5 cm^{-2} sec^{-1} (electrons). Below these thresholds, uncertainties due to variable noise levels require further analysis. Abbreviation: MP, magnetopause.

Table 1. Bow shock (BS) and magnetopause (MP) boundaries observed by the Voyager 2 PLS experiment. Solar wind measurements are as follows. Normal: $n = 0.025$ cm^{-3}, $V = 430$ km sec^{-1}, $T_p = 0.5$ eV; preshock: $n = 0.05$ cm^{-3}, $V = 450$ km sec^{-1}, $T_p = 4.7$ eV; outbound: $n = 0.05$ cm^{-3}, $V = 430$ km sec^{-1}, $T_p = 0.4$ eV (n, plasma density; V, velocity; T_p, proton temperature).

Boundary	Spacecraft event time (day/hour: minute)	Radial distance (R_U)	Distance from sun-planet line (R_U)
	Inbound pass		
BS	24/07:28	23.66	10.0
MP	24/10:08	18.04	8.7
	Outbound pass		
MP	26/07:15	80.56	42.9
BS(out)	27/22:06	160.7	89.7
BS(in)	27/23:03	162.8	90.9
BS(out)	28/02:37	170.2	95.2
BS(in)	28/02:46	170.7	95.4
BS(out)	28/03:15	171.6	95.9
BS(in)	28/03:19	171.6	95.9
BS(out)	28/13:00	192.0	107.9
BS(in)	28/21:27	209.7	118.2
BS(out)	28/21:50	210.7	118.8
BS(in)	28/21:55	210.7	118.8
BS(out)	29/03:00	221.2	124.9
BS(in)		Missing data	
BS(out)	29/06:00	227.4	128.5

dipole moment of 0.21 G R_U^3, a value that is in reasonable agreement with that inferred from Voyager MAG observations (0.23 G R_U^3) (*8*). Although the overall shape of the magnetosphere is consistent with a gas dynamic description, measurements at the bow shock reveal small-scale complexities. In particular, plasma parameters after the bow shock exhibit damped oscillations with a scale of roughly 0.5 R_U. Initial analysis of the data indicates that the observed plasma deceleration and heating are consistent with a perpendicular shock in a plasma with a high Mach number and a plasma β near 1.

Inner magnetosphere. The inner magnetosphere appears in the PLS measurements as the region of high particle intensities measured between 16 hours ($L = 7$ inbound) and 23 hours ($L = 18$ outbound) on 24 January. The color spectrogram in Fig. 3 shows the dramatic variations of the positive ion and electron spectra in this region. The particle distribution functions exhibit a complex structure that can be roughly described by three components: a warm population ($T \approx 10$ eV), a hot population ($T \approx 700$ eV to 3 keV), and a suprathermal tail to the warm protons (mean energy ≈ 50 to 100 eV). All the PLS measurements are consistent with the positive ions being protons corotating with the planet. There is no discernible signature of heavy ions (sputtered from the surfaces of the Uranian moons) or of α particles. In contrast to the plasma flows at Jupiter and Saturn, the inner magnetosphere flows are subsonic, and centrifugal forces are too weak to confine the plasma to low magnetic latitudes. The plasma energy density sampled by the PLS instrument is negligible compared to the energy density of the magnetic field ($\beta < 0.01$) throughout the inner magnetosphere. Alfvén Mach numbers calculated

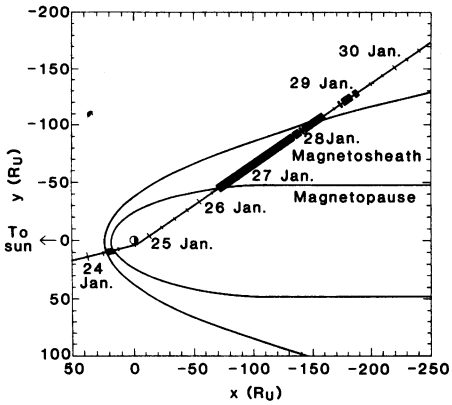

Fig. 2. Projection of the spacecraft trajectory onto the orbital plane of Uranus, with bow shock and magnetopause cross sections modeled from the observed crossings. The shading indicates regions where magnetosheath plasma was detected.

from a dipole field model (*8*) and densities consistent with our observations at the minimum L shells of the satellites Oberon (L_{min} = 22.9), Titania (L_{min} = 17.1), Umbriel (L_{min} = 10.4), Ariel (L_{min} = 7.5), and Miranda (L_{min} = 5.1) are 9×10^{-2}, 3×10^{-2}, 6×10^{-3}, 2×10^{-3}, and 3×10^{-3}, respectively.

Figure 4 shows the trajectory of Voyager 2 plotted in magnetic coordinates from the dipole field model of Ness and co-workers (*8*). This coordinate system would organize the plasma data if the inner magnetosphere were axially symmetric about the magnetic axis. The loop in the trajectory is a result of the large tilt angle between the magnetic and spin axes of the planet. The locations of seven features in the electron and positive-ion spectra that are indicative of changes in the plasma morphology are denoted in Figs. 1, 3, and 4 (key in legend to Fig. 4). Figures 1 and 3 show remarkable asymmetry in the plasma fluxes observed inbound and outbound. The PLS data indicate that the spacecraft moved through three regions separated by distinct boundaries at points 3 and 4. As Voyager 2 approached Uranus, the plasma fluxes began to rise soon after the spacecraft crossed Ariel's minimum L shell. The first indications of plasma were low fluxes of hot protons that were soon followed by a rise in electron density (point 1) and a sharp increase in total ion flux (point 2). In this region the densities of the hot and warm protons were comparable (up to about 0.5 cm^{-3}).

At the inbound plasma boundary (point 3; $L \approx 5.3$), the hot proton fluxes decreased by one order of magnitude in about 1 minute. Inside this boundary the warm proton fluxes fluctuated considerably (although overall the density continued to increase), reaching values of more than 2 cm^{-3} near closest approach. The proton temperature varied between 4 and 50 eV but showed no obvious trend with distance. In this innermost region, the electron fluxes decreased to very low levels; a plausible explanation would be that the electron temperature dropped well below the 10-eV energy threshold of the PLS instrument.

The outbound plasma boundary (point 4), inside Miranda's minimum L shell ($L \approx 4.8$), was characterized by a dramatic increase in fluxes of hot electrons (Fig. 3). The hot protons also reappeared at about this time. An intense flux of 2- to 4-keV electrons was encountered in the outbound region. This flux was apparently responsible for the spacecraft's acquiring a large negative potential (between points 5 and 6), which accelerated warm protons into the PLS detectors and produced the striking feature visible in Fig. 3. Energy cutoffs in the

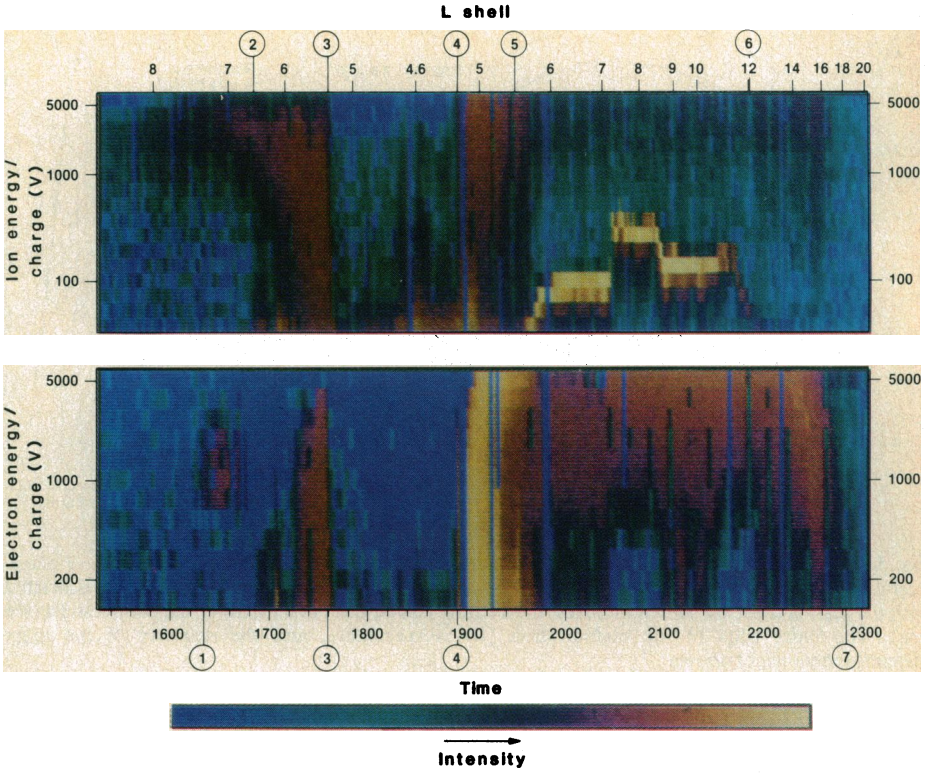

Fig. 3. Energy-time spectrograms of ion (top) and electron (bottom) intensities measured in the inner magnetosphere of Uranus. The logarithmic energy range spans 10 eV to 6 keV for ions and 120 eV to 6 keV for electrons. The color shading represents a logarithmic intensity scale, with the highest value measured shown in yellow. The circled numerals indicate features discussed in the text (key in legend to Fig. 4).

spectra indicate that the spacecraft potential reached −400 V during solar occultation. Although the charging ceased soon after the spacecraft came out of solar occultation (point 6), the hot electron flux persisted until point 7, where it suddenly dropped to background levels [as did the energetic particle fluxes observed by LECP (*9*) and CRS (*10*)]. Analysis of spectra in the charging region shows that there is no "hidden"

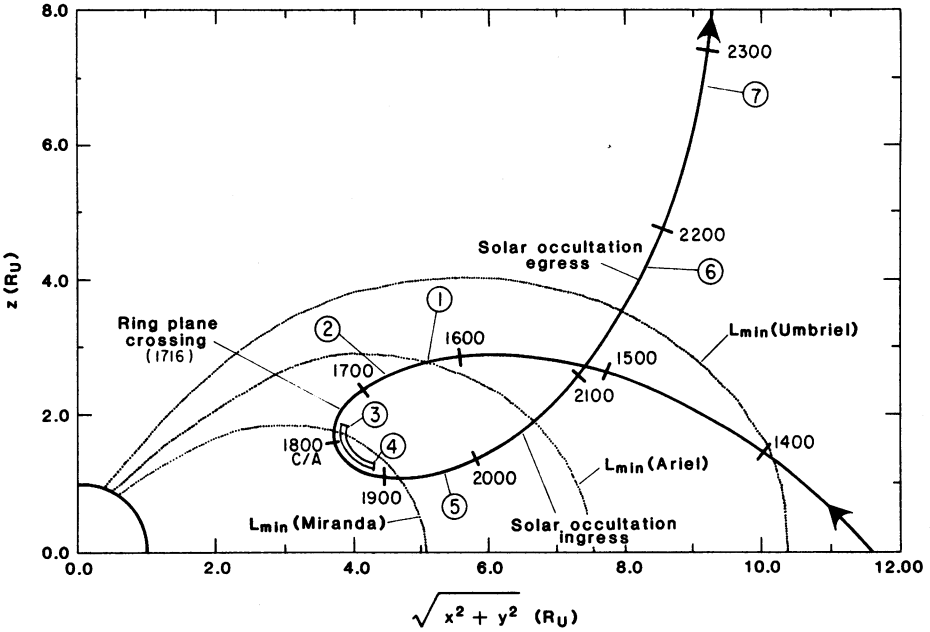

Fig. 4. Trajectory of the spacecraft in magnetic coordinates corresponding to the offset, tilted dipole model described by Ness and colleagues (*8*). The minimum magnetic L shells (L_{min}) of the satellites Miranda, Ariel, and Umbriel are shown. The circled numerals correspond to the following features: 1, electron density rise (1620 spacecraft event time); 2, ion flux increase (1650); 3, plasma edge (1736); 4, plasma edge (1854); 5, charging begins (1929); 6, charging ends (2152); 7, electron flux drop (2250).

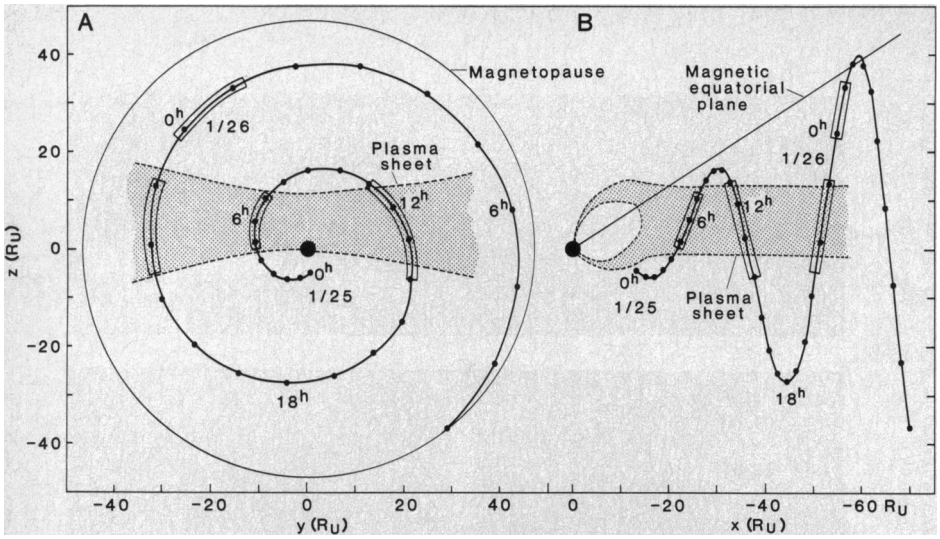

Fig. 5. Trajectory of Voyager 2 in solar magnetospheric coordinates. (A) y-z plane; (B) x-z plane. Positions of the spacecraft are marked every hour. Periods of enhanced electron intensities associated with the plasma sheet are shown in boxes; the shading corresponds to a model of the plasma sheet (see text). The inner edge of the plasma sheet (B) is speculative, and the structure of the inner magnetosphere is not shown.

thermal ion component below the normal energy range because the spacecraft charge would have accelerated such a population into the detectors.

Magnetotail and plasma sheet. As Voyager traversed the nightside outer magnetosphere, the PLS instrument repeatedly observed enhancements of electron and ion fluxes (Fig. 1). We interpret these enhancements to be passages of the spacecraft into or through the plasma sheet. By analogy with the magnetosphere of Earth, we expect the plasma sheet to form a quasi-planar structure in the center of the magnetotail. To the extent that the terrestrial analogy applies, the plasma sheet observations should be well organized in solar magnetospheric coordinates: x axis toward the sun, z axis defined so that the planet's magnetic dipole axis lies in the x-z plane, and y axis completing a right-handed set (we adopt the convention of terrestrial magnetosphere studies and let the magnetic dipole moment have a negative z component). Figure 5 shows the trajectory of Voyager 2 projected onto the solar magnetospheric y-z plane (a cross section of the magnetotail as viewed from the sun) and onto the x-z plane (the noon-midnight plane containing the solar wind flow vector and the planetary magnetic dipole). The portions of the trajectory where the total electron flux (in the energy range 140 eV to 6 keV) was enhanced are indicated.

The observations made before 0 hours on 26 January (spacecraft event time) are consistent with a simple model of the plasma sheet represented by the shading in Fig. 5: the plasma sheet has a full thickness of about 10 R_U near the midnight meridian that increases to about 15 R_U at the sides, and its central plane deviates from the magnetic equatorial plane to become parallel to the solar wind flow at tailward distances beyond 10 to 15 R_U. The plasma sheet is raised above the solar magnetospheric x-y plane as a result of the dipole tilt away from the z axis. The configuration and dimensions of this model largely correspond to a suitably scaled average model of the terrestrial plasma sheet. Because of the near-alignment of the Uranian spin axis and the solar wind flow during the present epoch, however, the structure does not wobble up and down as at Earth or Jupiter but instead rotates in space approximately about the x axis.

The observations made after 0 hours on 26 January are no longer consistent with the model described above: the plasma sheet (possibly not completely crossed) was observed between 0 and 1 hours, considerably above the expected position of the plasma sheet, and a crossing was not observed around 6 hours where it was expected. There are at least three possible explanations for the inconsistency: (i) because of the proximity of the magnetopause, there may be a tangential drag from the magnetosheath, tending to pull the plasma sheet up at the left and down at the right of Fig. 5 (in this figure, the magnetosheath plasma appears to rotate clockwise); (ii) the configuration may change markedly (as a result of a breakdown of corotation, for instance) at distances beyond about 55 R_U; or (iii) the configuration may undergo a major temporal change, possibly due to a change in solar wind direction, at about 0 hours.

Plasma sources and transport. In the magnetospheres of the rapidly rotating planets Jupiter and Saturn, the rotational motion of the plasma effectively prevents a systematic magnetospheric convection from penetrating the inner magnetosphere and allows radial plasma transport only by relatively slow diffusion processes. At Uranus, however, the near-alignment of the rotation axis with the direction of the solar wind results in a solar wind–driven magnetospheric convection system that transports plasma sunward throughout the magnetosphere (*12*). Scaling from the terrestrial magnetosphere (on the assumption of similar coupling mechanisms) would give a typical magnetospheric convection potential of 20 kV and an associated convection time scale of 40 hours (*1*). This or some other relatively rapid transport mechanism may explain why the moons of Uranus (unlike those of Saturn or Jupiter) do not appear to be significant sources of magnetospheric plasma: the heavy ions may be removed too quickly to allow a self-sustaining plasma torus to develop (*13*).

Another consequence of magnetospheric convection is that the solar wind may be a significant source of magnetospheric plasma. Protons of solar wind origin that are convected inward from the vicinity of the magnetopause or the magnetotail will be heated by adiabatic compression to nearly 30 keV, above the energy range of the PLS instrument. Solar wind electrons would be heated to a few kiloelectron volts by this process, which might be the source of the hot electrons observed on the night side of the inner magnetosphere.

Ionization of the extended neutral hydrogen corona observed around Uranus by the UVS experiment (*14*) constitutes an important and possibly the major source of plasma for the magnetosphere. Protons created from this source initially have the local rotational energy (0.4 eV at L = 5; 4 eV at L = 10), and their energy increases or decreases adiabatically with subsequent inward or outward transport. Thus the warm population of particles in the inner magnetosphere could result from nearly local formation and inward transport over a relatively small distance; in this case it is significant that the warm component is observed only at magnetic longitudes where the magnetospheric convection is expected to have an inward flow component (*12*) and is absent in the region where the convection should be outward. Alternatively, the warm population could be produced by strictly local ionization if there is a local mechanism for raising the proton temperature. The hot plasma population, if attributed to this source, must result from ionization of hydrogen at large L shells and subsequent adiabatic heating of the plasma as it is

transported to the inner magnetosphere.

Injection of particles from the ionosphere is another possible source of plasma. Precipitation of energetic charged particles into the ionosphere forms secondary electrons that should have energies of 20 to 40 eV and, by electrostatically pulling out ions, could provide an alternative source for the warm population. Similar processes have been discussed for other planets (*15*). Photoelectrons also have energies of 20 to 40 eV and are another possible source of plasma.

The boundary implied by the "plasma edge" observations ($L \approx 5$) can be interpreted in several ways. It may be the inner limit of magnetospheric convection due to residual effects of corotation associated with the small angle ($\approx 7°$) between Uranus' rotation axis and the solar wind (*12*) or to shielding by pressure gradient effects (*16*). The expected location of the convection limit in either case depends on presently unknown parameters, such as the ionospheric conductivity, but an L value of about 5 is not implausible. Alternatively, the boundary may be ascribed to plasma absorption by Miranda and its location related to Miranda's minimum L value, although the consistency with observations of the absorption signatures (including the predicted precise location) expected from this mechanism remains among the unsettled questions.

REFERENCES AND NOTES

1. G. L. Siscoe, *Icarus* **24**, 311 (1975).
2. T. W. Hill, A. J. Dessler, M. E. Rassbach, *Planet. Space Sci.* **31**, 1187 (1983).
3. A. K. Ip and G.-H. Voigt, *J. Geophys. Res.* **90**, 6287 (1985).
4. D. E. Shemansky and G. R. Smith, *Geophys. Res. Lett.* **13**, 1 (1986).
5. S. A. Curtis, *Nature (London)* **318**, 47 (1985).
6. A. Eviatar and J. D. Richardson, *Astrophys. J. Lett.* **301**, L99 (1985).
7. H. S. Bridge *et al.*, *Space Sci. Rev.* **21**, 259 (1977).
8. N. F. Ness *et al.*, *Science* **233**, 85 (1986).
9. S. M. Krimigis *et al.*, *ibid.*, p. 97.
10. E. C. Stone *et al.*, *ibid.*, p. 93.
11. J. A. Slavin *et al.*, *J. Geophys. Res.* **90**, 6275 (1985).
12. V. M. Vasyliunas, *Geophys. Res. Lett.*, in press.
13. J. D. Richardson, A. Eviatar, G. L. Siscoe, *J. Geophys. Res.*, in press.
14. A. L. Broadfoot *et al.*, *Science* **233**, 74 (1986).
15. R. M. Thorne, *Geophys. Res. Lett.* **8**, 509 (1981).
16. G. L. Siscoe, *J. Geophys. Res.* **87**, 5124 (1982).

17. We are deeply indebted to the many organizations and individuals who made the Voyager 2 Uranus encounter an outstanding scientific event. We especially thank the entire Voyager project staff at NASA Headquarters and at the Jet Propulsion Laboratory for their support of this and other Voyager experiments. We owe special thanks to O. Divers, B. McDougal, N. Toy, R. Hungerford, and E. Miner for assistance with encounter planning and operations; to A. Bowes, P. Milligan, J. Quigley, and G. Gordon for general support and for data reduction and analysis; to W. Mish and his colleagues for extensive and creative support throughout the encounter; to F. Kuykendall, S. Philipson, and their colleagues for extensive and invaluable color displays of our data; to D. Balcom for technical assistance; to the SUN Microsystems University Donation Program, whose support made rapid data analysis and color spectrograms possible; and to SUN staff M. Thomas for technical support and M. Moran, M. Goldstein, S. Stein, and J. Ablakat for arranging SUN's support. Supported by NASA under JPL Contract 953733.

31 March 1986; accepted 5 May 1986

Energetic Charged Particles in the Uranian Magnetosphere

E. C. STONE, J. F. COOPER, A. C. CUMMINGS, F. B. MCDONALD, J. H. TRAINOR, N. LAL, R. MCGUIRE,* D. L. CHENETTE

During the encounter with Uranus, the cosmic ray system on Voyager 2 measured significant fluxes of energetic electrons and protons in the regions of the planet's magnetosphere where these particles could be stably trapped. The radial distribution of electrons with energies of megaelectron volts is strongly modulated by the sweeping effects of the three major inner satellites Miranda, Ariel, and Umbriel. The phase space density gradient of these electrons indicates that they are diffusing radially inward from a source in the outer magnetosphere or magnetotail. Differences in the energy spectra of protons having energies of approximately 1 to 8 megaelectron volts from two different directions indicate a strong dependence on pitch angle. From the locations of the absorption signatures observed in the electron flux, a centered dipole model for the magnetic field of Uranus with a tilt of 60.1 degrees has been derived, and a rotation period of the planet of 17.4 hours has also been calculated. This model provides independent confirmation of more precise determinations made by other Voyager experiments.

THE VOYAGER 2 ENCOUNTER WITH Uranus revealed a moderate-sized magnetosphere surrounding this giant planet. Because the nature (or even the presence) of this magnetosphere was unknown before the encounter, the cosmic ray system (CRS) (*1*) was cycled every 192 seconds between two configurations to provide observations over a wide range of possible intensities of trapped particles. The instrument functioned normally throughout the encounter.

The trajectories at Uranus of the spacecraft, the satellites Miranda, Ariel, Umbriel, Titania, and Oberon, and the ϵ ring are shown in Fig. 1 in a magnetic coordinate system based on the offset tilted dipole model of the Uranian planetary magnetic field (*2*). The spacecraft crossed the magnetic equator once near 1321 spacecraft event time and reached a minimum L-shell value of 4.6 at 1829 (*3*). Because of the 60° tilt of the dipole relative to the rotation axis, the satellites sweep across broad ranges of L values and magnetic latitude as the planet rotates.

Electron spatial distributions. The electron absorption signatures of the three major inner satellites are shown in Fig. 2; these data were obtained from single detector counting rates of three detectors in the CRS instrument (*4*). The electron energy thresholds and detector geometric factors were estimated by analysis from the passive shielding surrounding each detector and from the energy deposit thresholds. The baseline counting rates of each detector were due to the interplanetary charged-particle background, primarily galactic cosmic rays. None of the counting rates displayed in Fig. 2 increased above background levels until Voyager 2 was well inside the magnetosphere. Rates from the highest electron energies rose above background only inside the orbit of Miranda. Although the spacecraft reached an L-shell value of only 4.6, the rapid increase in the intensity of high-energy electrons (≥ 7.6 MeV, curve 2 in Fig. 2) indicates an intense, high-energy radiation environment inside the region probed by Voyager 2.

At much lower electron energies, there are large spatial gradients in the magnetospheric flux in the outer magnetosphere (curve 1 in Fig. 3). Analysis of electronic pulse height data from the encounter and from calibrations after Voyager 2 was launched shows that this counting rate is dominated by the pile-up of low-energy (≥ 20 keV) electrons.

E. C. Stone, J. F. Cooper, A. C. Cummings, George W. Downs Laboratory of Physics, California Institute of Technology, Pasadena, CA 91125.
F. B. McDonald, NASA Headquarters, Washington, DC 20546.
J. H. Trainor, N. Lal, R. McGuire, Goddard Space Flight Center, Greenbelt, MD 20771.
D. L. Chenette, Aerospace Corporation, Los Angeles, CA 90009.

*Concurrent affiliation: Department of Physics and Astronomy, University of Maryland, College Park, MD 20742.